

Mechanism of CO Intercalation through the Graphene/Ni(111) Interface and Effect of Doping

Daniele Perilli, Sara Fiori, Mirco Panighel, Hongsheng Liu, Cinzia Cepek, Maria Peressi, Giovanni Comelli, Cristina Africh,* and Cristiana Di Valentin*



Cite This: <https://dx.doi.org/10.1021/acs.jpcllett.0c02447>



Read Online

ACCESS |



Metrics & More

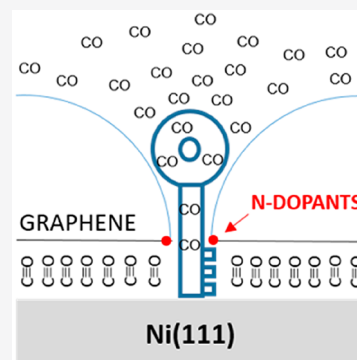


Article Recommendations



Supporting Information

ABSTRACT: Molecules intercalate at the graphene/metal interface even though defect-free graphene is impermeable to any atomic and molecular species in the gas and liquid phase, except hydrogen. The mechanism of molecular intercalation is still a big open question. In this Letter, by means of a combined experimental (STM, XPS, and LEED) and theoretical (DFT) study, we present a proof of how CO molecules succeed in permeating the graphene layer and get into the confined zone between graphene and the Ni(111) surface. The presence of N-dopants in the graphene layer is found to highly facilitate the permeation process, reducing the CO threshold pressure by more than an order of magnitude, through the stabilization of multiatomic vacancy defects that are the open doors to the bidimensional nanospace, with crucial implications for the catalysis under cover and for the graphene electrochemistry.



Molecule intercalation at the graphene (Gr)/metal (M) interface is a crucial process for several relevant applications, such as catalysis under cover,^{1–3} large-scale preparation of single-layer graphene from chemical vapor deposition (CVD),⁴ graphene-based electrochemistry⁵ and gas trapping in highly pressurized graphene nanobubbles.⁶

Several experimental proofs exist of the fact that gases succeed in reaching the confined zone beneath Gr.^{7–11} For example, scanning tunneling microscopy (STM) images reveal a change in the pattern when the gas intercalation decouples Gr from the substrate.⁸ Furthermore, molecular chemical reactivity under graphene is probed by real-time low-energy electron microscopy (LEEM)/photoemission electron microscopy (PEEM), X-ray photoelectron spectroscopy (XPS), and high-resolution electron energy loss (HREELS) spectroscopy.^{7,8,12}

However, gas or molecule intercalation still remains mostly an empirical observation: although crucial, the mechanism is not yet understood. It is even not yet established whether it is a general mechanism or it is molecule-dependent. Researchers can prove it occurs, but they do not really know how.

What it is clearly known is that defect-free Gr is impermeable to any atomic or molecular species in gas or liquid phase.¹³ Only the permeation of atomic and molecular hydrogen can be activated by the presence of some local curvature, due to a peculiar flipping mechanism, as recently reported.¹⁴ Then, an important open question, which we want to address in the present paper, is if Gr is impermeable, why do researchers observe gas intercalation at Gr/M interfaces?

One may expect that the mechanism of gas intercalation takes place in two main consecutive steps: (1) the gas permeation through the Gr layer; (2) the gas diffusion at the Gr/M interface away from the intercalation sites. The first step is determined by the gas permeability of Gr layers, which has been a topic of intense discussion in the past.¹⁵ The reason is that the ability to precisely control the quantity and location of molecular flux is of value in several graphene applications, such as molecular sieving membranes and sensor design, nanoscale 3D printing, and catalysis.^{16,17}

For large-sheet stacked graphene membranes, it has been established that gas permeation may take place by intercalation through structural defects, also known as the inner-sheet pathway, whose kinetics largely depends on their size and concentration.¹⁸ Discrete Ångström-sized pores, induced with a voltage pulse applied by a metallized atomic force microscope tip on a single graphene sheet, have also been used to control gas transport and selectivity in molecular valves.¹⁹

It is reasonable to expect that structural defects play a key role also for the intercalation of the gas molecules within Gr/M interfaces, as proposed in a recent experimental work.⁵

Received: August 10, 2020

Accepted: September 23, 2020

Published: September 23, 2020

66 Moreover, a theoretical study suggested that the presence of
67 dopants may influence graphene permeability.²⁰

68 In this work, through a combined theoretical and
69 experimental study, we propose a mechanism of CO
70 intercalation through a Gr/Ni(111) interface, based on density
71 functional theory calculations and consistent with the
72 experimental observations of CO exposure on pristine
73 graphene and N-doped graphene (N-Gr) grown on a
74 Ni(111) surface by low-energy electron diffraction (LEED),
75 XPS, and STM.

76 High-quality Gr and N-Gr layers on Ni(111) were grown by
77 low-pressure CVD.^{21,22} Carbon monoxide was then dosed at
78 pressures in the millibar regime (more details in the
79 experimental section in the Supporting Information). In the
80 LEED patterns obtained for pristine Gr (Figure 1a left), only
81 after exposure to 500 mTorr of CO, new extra spots, besides
82 the Ni and Gr markers, are visible, forming a pattern in line
83 with those reported in literature for CO on clean Ni(111) and
84 compatible with the coexistence of $c(4 \times 2)$ and $(\sqrt{7} \times$
85 $\sqrt{7})R19^\circ$ CO domains (nominal coverage of 0.5 and 0.57 ML,
86 respectively).^{23,24} On the other hand, for N-Gr (Figure 1b
87 left), new spots are present already after exposure to 20 mTorr
88 of CO, yielding one well-defined pattern corresponding to the
89 $(\sqrt{7} \times \sqrt{7})R19^\circ$ CO superstructure on clean Ni (nominal
90 coverage of 0.57 ML).^{23,24} On the basis of XPS and STM
91 results, we can rule out that CO is adsorbed on a residual clean
92 Ni region (not covered by Gr or N-Gr), implying that CO
93 intercalation underneath N-Gr occurs at a pressure that is
94 more than 1 order of magnitude lower than for pristine Gr.

95 XPS measurements carried out on Gr and N-Gr samples
96 before and after CO exposure (Figure 1a and 1b, right) present
97 features that confirm CO intercalation. In the C 1s spectrum,
98 two new components arise after CO exposure, suggesting a
99 detachment of the layer from the Ni substrate: the first one, at
100 283.6 eV, is characteristic of C from a Gr layer decoupled from
101 the metal substrate by intercalated CO;²⁵ the second one, at
102 285.3 eV, has been attributed to C from CO on Ni(111) in the
103 bridge position.²⁶ The same features are observed in the N-Gr
104 spectrum (Figure 1b right), but already after exposure at
105 significantly lower CO pressure.

106 We further confirm CO intercalation by STM. In Figure 2a,
107 the atomically resolved Gr layer imaged before CO exposure
108 shows the two triangular sublattices typical of the top-fcc
109 arrangement.²¹ Due to the strong Gr/Ni interaction, the C
110 atoms on fcc positions are imaged brighter than those on top,
111 in agreement with density functional theory (DFT) simu-
112 lations (Figure 2d). In Figure 2b, after CO intercalation below
113 Gr, the whole hexagon of the honeycomb lattice appears with
114 uniform intensity, in agreement with the simulated STM image
115 in Figure 2e. The presence of an intercalated buffer layer
116 affects also the appearance of N-related structures in N-Gr, as
117 evident in Figure 2c for one of the most abundant defects
118 observed on the N-Gr/CO/Ni(111) surface. The bright
119 protrusion at the center is surrounded by a $\sqrt{3} \times \sqrt{3}$ pattern,
120 not present before CO intercalation,²² which we ascribe to the
121 typical quantum interference pattern due to scattering by one
122 or more C vacancies in a Gr layer that is weakly interacting
123 with the substrate.²⁷ This defect is a 3N pyridinic species, as
124 unambiguously confirmed by the simulated STM image in
125 Figure 2f.

126 Thus, the morphological and chemical characterization of
127 pristine Gr and N-Gr yields very similar results with all the
128 applied techniques (both at the atomic scale with STM as well

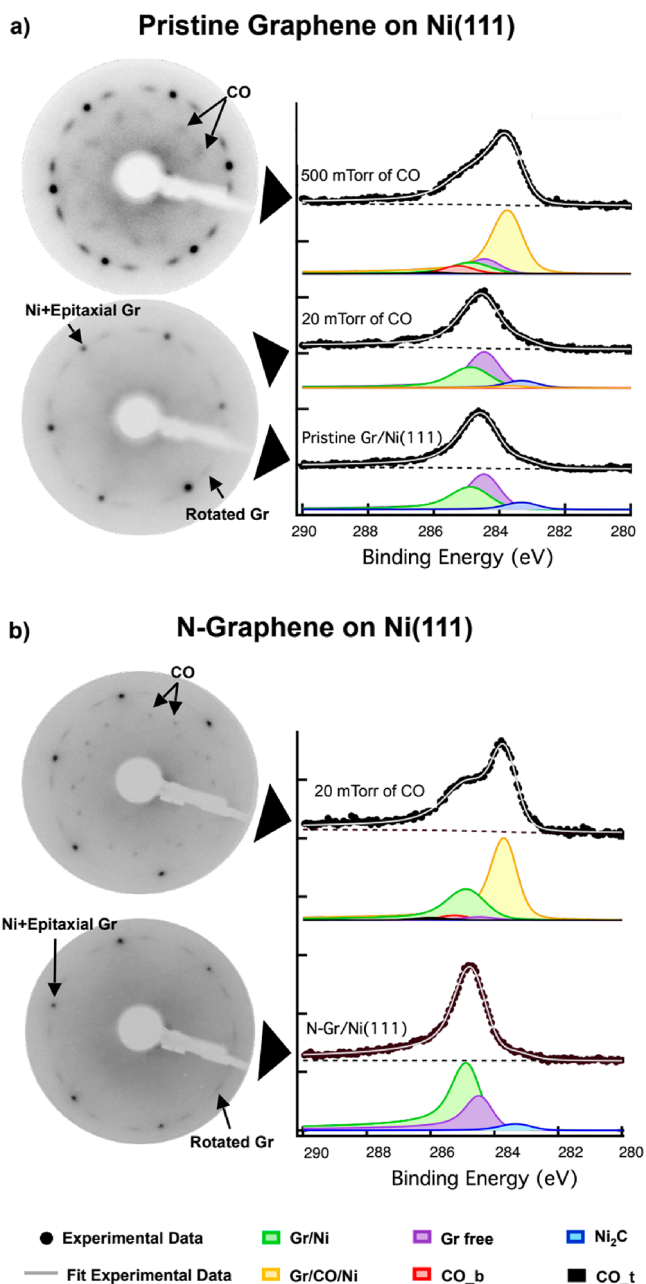


Figure 1. LEED patterns and XPS spectra of (a) pristine Gr and (b) N-Gr on Ni(111) substrates before and after CO exposure in the millibar regime. The colors of the different XPS components correspond to green, Gr interacting with Ni; purple, Gr not interacting with Ni (Ni carbide underneath Gr); blue, Ni carbide; yellow, Gr interacting with CO (CO underneath Gr); red and black, CO on Ni(111) in bridge and top positions, respectively.

as by integrating methods like LEED and XPS), with the only
crucial difference being the threshold pressure required to
induce CO intercalation and Gr decoupling: 500 mTorr vs
20 mTorr, respectively.

The next question to answer is how did CO molecules get
through the graphene layer and reach the Gr/Ni(111)
interface? Since even H_2 , the smallest molecule in nature,
graphene must be impermeable to CO molecules. Therefore,
reasonably, there must be some vacancies in the graphene
lattice. How big should these “holes” be to allow a CO

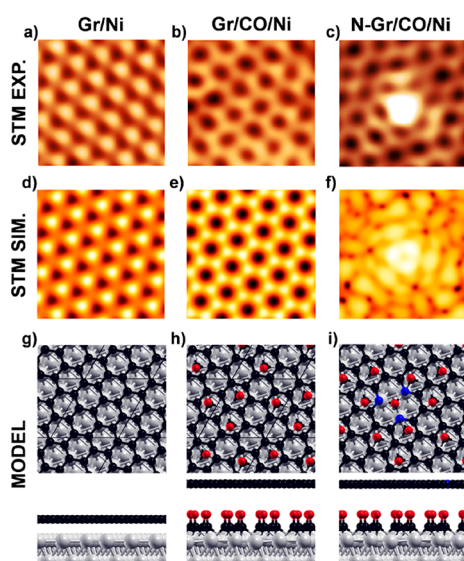


Figure 2. Pristine and N-doped Gr/Ni interfaces with and without intercalated CO molecules at 0.57 ML coverage. Experimental (panels a–c) and DFT simulated (panels d–f) STM images. Image size: $1.2 \times 1.2 \text{ nm}^2$. Experimental parameters: (a) $I = 0.1 \text{ nA}$, $V_{\text{bias}} = -0.3 \text{ V}$; (b) $I = 0.7 \text{ nA}$, $V_{\text{bias}} = -0.2 \text{ V}$; (c) $I = 0.98 \text{ nA}$, $V_{\text{bias}} = -0.05 \text{ V}$. Computational parameters: (d, e) $V_{\text{bias}} = -0.2 \text{ V}$, ILDOS isosurface lying at 2 \AA above graphene; (f) $V_{\text{bias}} = -0.05 \text{ V}$, ILDOS iso-surface lying $\approx 3 \text{ \AA}$ above graphene and with ILDOS value of $1 \times 10^{-5} |e|/a_0^3$. Panels (g)–(i): ball-and-stick models of the DFT relaxed structures (top and side views). Color coding: Ni atoms in gray, C atoms in black, O atoms in red, and N atoms in blue.

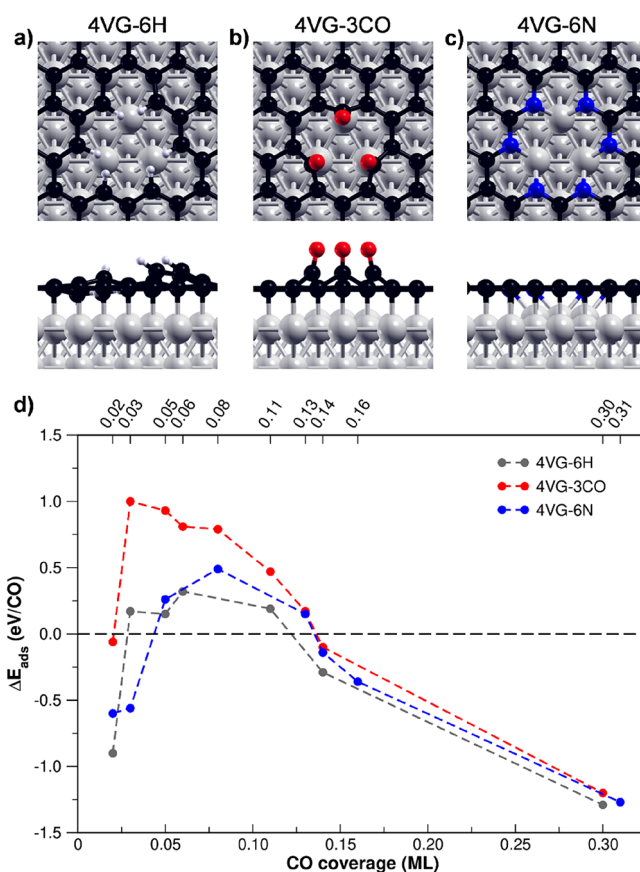


Figure 3. Top and side views for the three models of vacancy considered: (a) 4VG-6H, (b) 4VG-3CO, and (c) 4VG-6N. Color coding: Ni atoms in gray, C atoms in black, H atoms in light gray, O atoms in red, and N atoms in blue. (d) Energy profile (normalized by the number of CO molecules) for the CO adsorption as a function of the CO coverage for each of the vacancy models: 4VG-6H, 4VG-3CO, and 4VG-6N (gray, red, and blue line, respectively). Values of the coverages represented by the dots in the curves are reported on the top x-axis. The ball-and-stick representations of the structures at different CO coverage for 4VG-6N are shown in Figure S4.

140 molecule to pass? Then, why is it so much easier to reach the
141 interface when Gr is doped with N?

142 The most common atomic defect in pristine Gr/Ni(111) is
143 known to be a triatomic C vacancy trapping a Ni adatom
144 (1Ni@3VG).²⁸ However, this seems to not be the gate for
145 intercalation: if we model a CO molecule on top of it, the C
146 atom is found to fill one of the vacancies whereas O becomes
147 very tightly bound to Ni. When we add a second CO molecule,
148 we observe the formation of CO₂ with one C left in the defect
149 (Figure S1). In the case of N-Gr/Ni(111), the most common
150 atomic defect is a C monovacancy surrounded by three
151 pyridinic N atoms, as discussed above.²² The adsorption of one
152 CO in this C vacancy is however very unstable (by $\sim 3 \text{ eV}$),
153 because the defect is too small to accommodate it (Figure S2).

154 Therefore, one crucial aspect for the CO permeation
155 through the graphene layer appears to be the critical size of
156 the atomic holes allowing the molecules to pass through. Since
157 the triatomic vacancy is found not to be suitable, we have
158 investigated a tetra-atomic vacancy. The undercoordinated C
159 atoms surrounding the vacancy are very reactive and therefore
160 either they bind to the underlying Ni substrate, blocking the
161 passage of the molecules into the confined zone between the
162 Gr and the Ni(111) surface,²⁹ or they might react with residual
163 hydrogen gas present in the chamber forming CH bonds³⁰ or
164 directly with the dosed CO molecules. These reactions yield
165 the two configurations shown in Figure 3a and b. Instead, for
166 the case of defective N-Gr, we have found that N atoms tend
167 to diffuse and segregate to the defect edges, where they
168 become pyridinic.²² In other words, there is a downhill slope in
169 energy, which favors the concentration of pyridinic N at the
170 defect edges, passivating the defect toward reactivity with H₂
171 or CO. By simply comparing the structures of the three types

of holes in Figure 3a–c (4VG-6H, 4VG-3CO, and 4VG-6N),
there is an evident obstruction of the hole for 4VG-3CO,
whereas 4VG-6N appears to be the largest, with no steric
hindrance. Moreover, the N atoms at the edges are much less
strongly bound to the underlying Ni substrate than unsaturated
C atoms.

We will focus the attention on the 4VG-3CO and 4VG-6N
models, which, at variance with the 4VG-6H model, do not
require dissociation of gas phase molecules for their formation.
More specifically, we have investigated the energy profile for
one CO molecule to vertically enter the atomic hole, by
moving the CO molecule along the z-direction and, at each
different CO height, allowing all the atoms to fully relax. The
two energy profiles for 4VG-3CO and for 4VG-6N, reported in
Figure S3, are extremely different: for 4VG-3CO, the energy
goes up to almost 5 eV when the distance of CO from the Ni
surface is 2.6 Å, whereas for 4VG-6N it reaches a value of only
0.19 eV, which represents a rough estimation of the activation
barrier. On this basis, we can draw an important conclusion:
N-doping causes a chemical stabilization of multivacancies in
Gr, which results in much less sterically hindered atomic holes
in the 2D network, thus facilitating molecule permeation. We
expect this to have a tremendous effect on the threshold

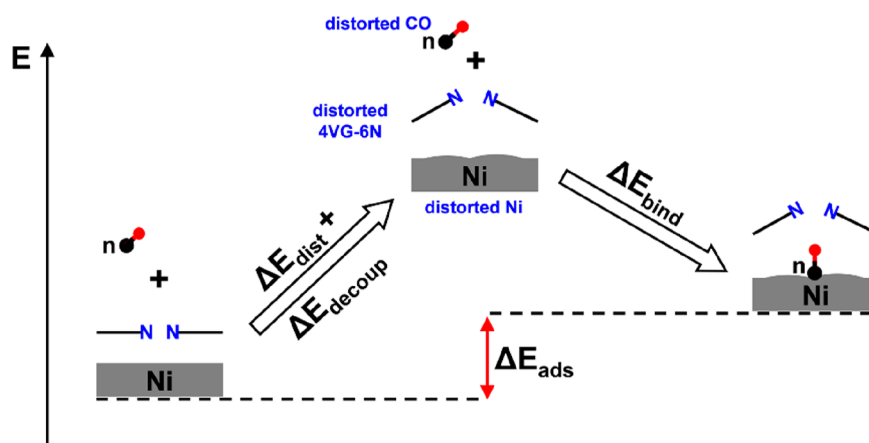


Figure 4. Schematic representation of the energy decomposition analysis for the energy contribution of distortion (positive, ΔE_{dist}), decoupling (positive, ΔE_{decoup}), and binding (negative, ΔE_{bind}) to the adsorption energy (ΔE_{ads}) of CO at the interface between N-doped graphene (4VG-6N) and Ni(111) surface. All the energy contributions are normalized by the number of CO molecules.

195 pressure for CO intercalation, as we will discuss in the
196 following.

197 For both 4VG-3CO and 4VG-6N, our calculations show that
198 the first CO molecule is favorably bound to the Ni surface, by
199 -0.06 and -0.60 eV, respectively. As a further step in our
200 mechanistic study, we have added other CO molecules, one at
201 a time, and analyzed the variation in energy as normalized to
202 the number of added CO molecules (see Figure 3d). We did
203 this for all the three “hole” models. The three curves are quite
204 different in the first part of the graph, but they tend to line up
205 in the second part, above 0.11 ML. 4VG-6N presents an
206 energy profile which never exceeds 0.5 eV and is very similar to
207 the one of 4VG-6H, where we do not expect any strong
208 interaction of the CH groups with the underlying Ni substrate.
209 This means that, for 4VG-6N, it is not too energetically
210 demanding for one CO molecule at a time not only to go
211 through the hole (see Figure S3), but also to intercalate in the
212 confined zone between the Gr layer and the Ni surface (see
213 Figure 3d). This is because the N atoms are not strongly
214 interacting with the substrate and therefore can be lifted at a
215 reasonable cost to facilitate the CO passage. All the structures
216 at different CO coverages for 4VG-6N are shown in Figure S4.
217 The highest energy value (~ 0.5 eV) is registered at 0.08 ML
218 coverage, then the curve starts to slope down. Very
219 interestingly, at the turn between 0.13 and 0.14 ML, we
220 observe a twist in the energy, going to negative values. In other
221 words, from 0.14 ML onward, there is an energy gain for each
222 additional CO molecule. This twist is actually observed at 0.14
223 ML for all the models of multivacancy considered, thus
224 suggesting that something special occurs at this coverage.

225 Some important insight on this issue comes from a similar
226 analysis, performed for a nondefective Gr layer on the Ni(111)
227 substrate and reported in Figure S5. Even in this case, where
228 no defect is present in the Gr lattice, we observe that the cost
229 to have CO molecules in the confined zone between the two
230 materials reduces with the number of added molecules, turning
231 into an energy gain for coverages ≥ 0.14 ML. Therefore, 0.14
232 ML corresponds to the critical point when the cost to detach
233 the Gr layer from the Ni substrate is counterbalanced and even
234 overcome by the gain of establishing a certain amount of Ni–
235 CO bonds.

236 We have performed an energy decomposition analysis for
237 4VG-6N to establish the exact contributions from (1) the cost

to decouple Gr/Ni(111) (ΔE_{decoup}); (2) the cost to distort 238
Gr/Ni(111) to accommodate the CO molecules (ΔE_{dist}); (3) 239
the binding energy for the Ni–CO bonds (ΔE_{bind}). The first 240
two terms are energy costs, whereas the third one is an energy 241
gain, as shown in Figure 4 and detailed in Table 1. We carried 242 f4t1

Table 1. Energy Contributions of the Energy Decomposition Analysis for CO Adsorption on 4VG-6N of Distortion (Positive, ΔE_{dist}), Decoupling (Positive, ΔE_{decoup}), and Binding (Negative, ΔE_{bind}) to the Adsorption Energy (ΔE) at Different CO Coverages^a

CO coverage (ML)	ΔE_{ads} (eV/CO)	ΔE_{dist} (eV/CO)	ΔE_{decoup} (eV/CO)	ΔE_{bind} (eV/CO)
0.03	-0.56	+0.43	+0.59	-1.58
0.05	+0.26	+1.45	+0.44	-1.63
		+1.02	-0.15	-0.05
0.13	+0.15	+0.08	+2.66	-2.59
0.14	-0.14	+0.04	+2.42	-2.61
		-0.04	-0.24	-0.02

^aAll terms are normalized to the number of CO molecules (eV/CO). Total energy differences are reported in Table S1. The energy contributions are calculated using as a reference the optimized 4VG-6N interface and isolated CO molecules in the gas-phase.

out this analysis at the two critical coverages where there is an 243
inversion in the energy balance: gain/cost at 0.03/0.05 ML and 244
cost/gain at 0.13/0.14 ML (see Figure 3d). We observe that 245
going from 0.03 to 0.05 ML there is a large increase in the 246
energy cost of distortion (+1.02 eV/CO) but a small reduction 247
in the cost for decoupling (-0.15 eV/CO), whereas the energy 248
gain due to CO binding per molecule is about the same 249
(difference of only -0.05 eV/CO). On the contrary, going 250
from 0.13 to 0.14 ML, we observe a small decrease both in the 251
energy cost of distortion (-0.04 eV/CO) and of decoupling 252
(-0.24 eV/CO) with a similar energy gain of binding per CO 253
molecule (-0.02 eV/CO). 254

Another important aspect of the intercalation mechanism is 255
related to the role played by the CO molecules distribution on 256
the surface. We assumed that in the initial phase most of the 257
CO molecules are close to the multiaatomic hole through which 258
they have reached the Ni surface; then, they gradually diffuse 259
under the Gr layer and become more equally distributed on 260
the surface. We have verified that this picture is compatible 261

262 with the energy costs involved. First, we have compared the
 263 stabilization energy at 0.14 ML for two different CO
 264 distributions for 4VG-6N, as shown in Figure S6: (a) close
 265 to the hole edges and (b) more equally distributed beneath the
 266 interface. From (a) to (b), there is an energy gain per CO
 267 molecule of -0.044 eV ($\times 9$ CO = -0.40 eV), which indicates
 268 a driving force for the CO molecules to better distribute,
 269 reducing their repulsive interaction. We estimated the
 270 activation barrier for the CO diffusion in the confined zone
 271 between Ni(111) and Gr through a nudged elastic band
 272 (NEB) calculation to be 0.19 eV (Figure S7), which is very
 273 close to that computed for the corresponding process on the
 274 bare Ni(111) surface, experimentally observed already at 130
 275 K, which is 0.15 eV.^{31,32}

276 Finally, we prove by means of STM that defects with a size
 277 comparable to 4VG are rare in pristine Gr whereas they are
 278 often visualized on the N-Gr surface, both at the grain
 279 boundaries and in between the N-Gr domains. Figure 5a

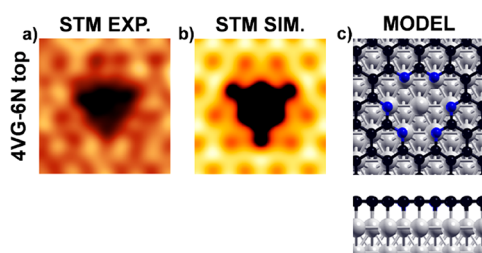


Figure 5. (a) Experimental and (b) simulated STM images of the 4VG-6N top configuration. (c) Ball-and-stick model in top and side view. Experimental parameters: (a) $I = 1.4$ nA, $V_{\text{bias}} = -0.2$ V. Computational parameters: $V_{\text{bias}} = -0.2$ V; ILDOS iso-surface lying ≈ 2 Å above graphene and with ILDOS value of 5×10^{-5} $|e|/a_0^3$. Color coding: Ni atoms in gray, C atoms in black, and N atoms in blue.

280 reports an atomic scale image of a typical large defect present
 281 on the N-Gr/Ni(111) layer. It appears as a big dark triangular
 282 feature, which suggests a multiatomic vacancy. This large
 283 defect is remarkably well reproduced by the simulated STM
 284 image of a tetra-atomic vacancy with edges decorated by six N
 285 atoms in the top positions (Figure 5b), thus differing from the
 286 4VG-6N model proposed above only for the registry with the
 287 substrate.

288 In conclusion, our work, based on the synergic contribution
 289 of DFT calculations and LEED, XPS, and STM experiments,
 290 has unraveled and given proof of the mechanism of CO
 291 intercalation at the Gr/Ni interface, which is highly facilitated
 292 by the presence of N-dopants, stabilizing multiatomic vacancy
 293 defects and turning them in narrow open doors to the confined
 294 zone between the two materials. Similar mechanisms are likely
 295 to apply to other cases of molecular intercalation at the Gr/M
 296 interface, where the process has been observed but not yet
 297 explained. The next challenge is to assess to what extent the
 298 mechanism we have proposed is a general one, which will
 299 require a systematic investigation considering other gases and
 300 different dopants. A clear solution to this puzzle is a crucial
 301 step toward engineering the Gr/M interface in order to design
 302 and realize systems with tailored properties for practical
 303 applications.

ASSOCIATED CONTENT

Supporting Information

The Supporting Information is available free of charge at
<https://pubs.acs.org/doi/10.1021/acs.jpcllett.0c02447>.

Computational details, experimental details, reaction
 path of CO at 1Ni@3VG, models of CO adsorption of
 3N^{PPT}, energy profile of CO approaching 4VG-3CO and
 4VG-6N, models of intercalated CO in 4VG-6N at
 different CO coverage, energy profile of intercalated CO
 in Gr/Ni(111) at different CO coverage, two different
 CO distributions at 0.14 ML for 4VG-6N, energy profile
 for CO diffusion in the Gr/Ni(111) interface, energy
 decomposition analysis based on total energies (PDF)

AUTHOR INFORMATION

Corresponding Authors

Cristina Africh – CNR-IOM, Laboratorio TASC, 34149
 Trieste, Italy; orcid.org/0000-0002-1922-2557;
 Email: africh@iom.cnr.it

Cristiana Di Valentin – Dipartimento di Scienza dei Materiali,
 Università di Milano-Bicocca, I-20125 Milano, Italy;
orcid.org/0000-0003-4163-8062;
 Email: cristiana.divalentin@unimib.it

Authors

Daniele Perilli – Dipartimento di Scienza dei Materiali,
 Università di Milano-Bicocca, I-20125 Milano, Italy

Sara Fiori – CNR-IOM, Laboratorio TASC, 34149 Trieste,
 Italy; Department of Physics, University of Trieste, 34127
 Trieste, Italy

Mirco Panighel – CNR-IOM, Laboratorio TASC, 34149
 Trieste, Italy

Hongsheng Liu – Dipartimento di Scienza dei Materiali,
 Università di Milano-Bicocca, I-20125 Milano, Italy;
 Laboratory of Materials Modification by Laser, Ion and
 Electron Beams, Dalian University of Technology, Ministry of
 Education, Dalian 116024, China

Cinzia Cepek – CNR-IOM, Laboratorio TASC, 34149 Trieste,
 Italy

Maria Peressi – Department of Physics, University of Trieste,
 34127 Trieste, Italy; orcid.org/0000-0001-6142-776X

Giovanni Comelli – CNR-IOM, Laboratorio TASC, 34149
 Trieste, Italy; Department of Physics, University of Trieste,
 34127 Trieste, Italy; orcid.org/0000-0003-4603-2094

Complete contact information is available at:

<https://pubs.acs.org/doi/10.1021/acs.jpcllett.0c02447>

Author Contributions

D.P. and S.F. have contributed equally to this work.

Notes

The authors declare no competing financial interest.

ACKNOWLEDGMENTS

This work has been supported by the project “MADAM -
 Metal Activated 2D cArbon-based platforMs” funded by the
 MIUR Progetti di Ricerca di Rilevante Interesse Nazionale
 (PRIN) Bando 2017 - Grant 2017NYPHN8.

REFERENCES

- (1) Jin, L.; Fu, Q.; Dong, A.; Ning, Y.; Wang, Z.; Bluhm, H.; Bao, X. Surface chemistry of CO on Ru (0001) under the confinement of 359 graphene cover. *J. Phys. Chem. C* **2014**, *118*, 12391–12398. 360

- (2) Fu, Q.; Bao, X. Surface chemistry and catalysis confined under two-dimensional materials. *Chem. Soc. Rev.* **2017**, *46*, 1842–1874.
- (3) Li, H.; Xiao, J.; Fu, Q.; Bao, X. Confined catalysis under two-dimensional materials. *Proc. Natl. Acad. Sci. U. S. A.* **2017**, *114*, 5930–5934.
- (4) Ma, D.; Zhang, Y.; Liu, M.; Ji, Q.; Gao, T.; Zhang, Y.; Liu, Z. Clean transfer of graphene on Pt foils mediated by a carbon monoxide intercalation process. *Nano Res.* **2013**, *6*, 671–678.
- (5) Palacio, I.; Otero-Irurueta, G.; Alonso, C.; Martínez, J. I.; López-Elvira, E.; Muñoz-Ochando, I.; Salavagione, H. J.; López, M. F.; García-Hernandez, M.; Méndez, J.; Ellis, G. J.; Martín Gago, J. A. Chemistry below graphene: Decoupling epitaxial graphene from metals by potential-controlled electrochemical oxidation. *Carbon* **2018**, *129*, 837–846.
- (6) Zahra, K. M.; Byrne, C.; Alieva, A.; Casiraghi, C.; Walton, A. S. Intercalation, decomposition, entrapment—a new route to graphene nanobubbles. *Phys. Chem. Chem. Phys.* **2020**, *22*, 7606–7615.
- (7) Mu, R.; Fu, Q.; Jin, L.; Yu, L.; Fang, G.; Tan, D.; Bao, X. Visualizing chemical reactions confined under graphene. *Angew. Chem., Int. Ed.* **2012**, *51*, 4856–4859.
- (8) Granas, E.; Andersen, M.; Arman, M. A.; Gerber, T.; Hammer, B.; Schnadt, J.; Andersen, J. N.; Michely, T.; Knudsen, J. CO intercalation of graphene on Ir (111) in the millibar regime. *J. Phys. Chem. C* **2013**, *117*, 16438–16447.
- (9) Wei, M.; Fu, Q.; Yang, Y.; Wei, W.; Crumlin, E.; Bluhm, H.; Bao, X. Modulation of surface chemistry of CO on Ni (111) by surface graphene and carbidic carbon. *J. Phys. Chem. C* **2015**, *119*, 13590–13597.
- (10) Silva, C. C.; Cai, J.; Jolie, W.; Dombrowski, D.; Farwick zum Hagen, F. H.; Martínez-Galera, A. J.; Schlueter, C.; Lee, T.-L.; Busse, C. Lifting Epitaxial Graphene by Intercalation of Alkali Metals. *J. Phys. Chem. C* **2019**, *123*, 13712–13719.
- (11) Petrović, M.; Rakić, I. Š.; Runte, S.; Busse, C.; Sadowski, J. T.; Lazić, P.; Pletikosić, I.; Pan, Z.-H.; Milun, M.; Pervan, P.; Atodiresi, N.; Brako, R.; Šokčević, D.; Valla, T.; Michely, T.; Kralj, M. The mechanism of caesium intercalation of graphene. *Nat. Commun.* **2013**, *4*, 2772.
- (12) He, G.; Wang, Q.; Yu, H. K.; Farias, D.; Liu, Y.; Politano, A. Water-induced hydrogenation of graphene/metal interfaces at room temperature: Insights on water intercalation and identification of sites for water splitting. *Nano Res.* **2019**, *12*, 3101–3108.
- (13) Bunch, J. S.; Verbridge, S. S.; Alden, J. S.; Van Der Zande, A. M.; Parpia, J. M.; Craighead, H. G.; McEuen, P. L. Impermeable atomic membranes from graphene sheets. *Nano Lett.* **2008**, *8*, 2458–2462.
- (14) Sun, P. Z.; Yang, Q.; Kuang, W. J.; Stebunov, Y. V.; Xiong, W. Q.; Yu, J.; Nair, R. R.; Katsnelson, M. I.; Yuan, S. J.; Grigorieva, I. V.; Lozada-Hidalgo, M.; Wang, F. C.; Geim, A. K. Limits on gas impermeability of graphene. *Nature* **2020**, *579*, 229–232.
- (15) Yoon, H. W.; Cho, Y. H.; Park, H. B. Graphene-based membranes: status and prospects. *Philos. Trans. R. Soc., A* **2016**, *374*, 20150024.
- (16) Kim, H. W.; Yoon, H. W.; Yoon, S.-M.; Yoo, B. M.; Ahn, B. K.; Cho, Y. H.; Shin, H. J.; Yang, H.; Paik, U.; Kwon, S.; Choi, J.-Y.; Park, H. B. Selective gas transport through few-layered graphene and graphene oxide membranes. *Science* **2013**, *342*, 91–95.
- (17) Pierleoni, D.; Minelli, M.; Ligi, S.; Christian, M.; Funke, S.; Reineking, N.; Morandi, V.; Doghieri, F.; Palermo, V. Selective gas permeation in graphene oxide-polymer self-assembled multilayers. *ACS Appl. Mater. Interfaces* **2018**, *10*, 11242–11250.
- (18) Ibrahim, A.; Lin, Y. S. Gas permeation and separation properties of large-sheet stacked graphene oxide membranes. *J. Membr. Sci.* **2018**, *550*, 238–245.
- (19) Wang, L.; Drahushuk, L. W.; Cantley, L.; Koenig, S. P.; Liu, S.; Pellegrino, J.; Strano, M. S.; Bunch, J. S. Molecular valves for controlling gas phase transport made from discrete ångström-sized pores in graphene. *Nat. Nanotechnol.* **2015**, *10*, 785–790.
- (20) Mallineni, S. S. K.; Boukhvalov, D. W.; Zhidkov, I. S.; Kukharenko, A. I.; Slesarev, A. I.; Zatsepin, A. F.; Cholakh, S. O.; Rao, A. M.; Serkiz, S. M.; Bhattacharya, S.; Kurmaev, E. Z.; Podila, R. Influence of dopants on the impermeability of graphene. *Nanoscale* **2017**, *9*, 6145–6150.
- (21) Bianchini, F.; Patera, L. L.; Peressi, M.; Africh, C.; Comelli, G. Atomic scale identification of coexisting graphene structures on Ni (111). *J. Phys. Chem. Lett.* **2014**, *5*, 467–473.
- (22) Fiori, S.; Perilli, D.; Panighel, M.; Cepek, C.; Ugolotti, A.; Sala, A.; Liu, H.; Comelli, G.; Di Valentin, C.; Africh, C. “Inside Out” Growth Method for High-Quality Nitrogen-Doped Graphene. *arXiv (Materials Science)*, September 21, 2020, 2009.09789, ver. 1. <http://arxiv.org/abs/2009.09789>.
- (23) Campuzano, J. C.; Dus, R.; Greenler, R. G. The sticking probability, dipole moment, and absolute coverage of CO on Ni (111). *Surf. Sci.* **1981**, *102*, 172–184.
- (24) Erley, W.; Besocke, K.; Wagner, H. Absolute coverage determination of CO on Ni (111). *J. Chem. Phys.* **1977**, *66*, 5269–5273.
- (25) Wei, M.; Fu, Q.; Yang, Y.; Wei, W.; Crumlin, E.; Bluhm, H.; Bao, X. Modulation of surface chemistry of CO on Ni (111) by surface graphene and carbidic carbon. *J. Phys. Chem. C* **2015**, *119*, 13590–13597.
- (26) Held, G.; Schuler, J.; Sklarek, W.; Steinrück, H. P. Determination of adsorption sites of pure and coadsorbed CO on Ni (111) by high resolution X-ray photoelectron spectroscopy. *Surf. Sci.* **1998**, *398*, 154–171.
- (27) Mallet, P.; Varchon, F.; Naud, C.; Magaud, L.; Berger, C.; Veuillen, J. Y. Electron states of mono- and bilayer graphene on SiC probed by scanning-tunneling microscopy. *Phys. Rev. B: Condens. Matter Mater. Phys.* **2007**, *76*, 041403.
- (28) Carnevali, V.; Patera, L. L.; Prandini, G.; Jugovac, M.; Modesti, S.; Comelli, G.; Peressi, M.; Africh, C. Doping of epitaxial graphene by direct incorporation of nickel adatoms. *Nanoscale* **2019**, *11*, 10358–10364.
- (29) Dong, A.; Fu, Q.; Wu, H.; Wei, M.; Bao, X. Factors controlling the CO intercalation of h-BN overlayers on Ru (0001). *Phys. Chem. Chem. Phys.* **2016**, *18*, 24278–24284.
- (30) Patera, L. L.; Bianchini, F.; Troiano, G.; Dri, C.; Cepek, C.; Peressi, M.; Africh, C.; Comelli, G. Temperature-driven changes of the graphene edge structure on Ni (111): Substrate vs hydrogen passivation. *Nano Lett.* **2015**, *15*, 56–62.
- (31) Zhu, X. D.; Rasing, T.; Shen, Y. R. Surface diffusion of CO on Ni (111) studied by diffraction of optical second-harmonic generation off a monolayer grating. *Phys. Rev. Lett.* **1988**, *61*, 2883.
- (32) Lin, T. S.; Lu, H. J.; Gomer, R. Diffusion of CO on Ni (111) and Ni (115). *Surf. Sci.* **1990**, *234*, 251–261.